Free-Flight Rocket's Initial Trajectory as Affected by Massive Blowby

Daniel W. Barnette* and John J. Bertin†
The University of Texas at Austin, Austin, Texas
and
James L. Batson‡
Redstone Arsenal, Huntsville, Ala.

An experimental program has been conducted to determine the unbalanced forces on a tube-launched rocket due to the choking and the subsequent reversal (or blowby) of the exhaust flow. An underexpanded jet of unheated air was exhausted into a nontipoff launch tube. The surface of the simulated rocket was instrumented with static pressure orifices, located in diametrically opposed pairs. The differential pressure measurements were used to compute the rocket's trajectory in a three-degree-of-freedom program. Relatively large asymmetric pressure differentials were measured on the surface of the simulated rocket. Although the lateral displacement of the rocket was relatively insensitive to these pressure differentials, they caused large oscillatory variations in the pitch angle and in the pitch rate.

Nomenclature

A = cross-sectional area
F_x, F_y = forces measured with respect to the x and y axes, respectively
I_z = moment of inertia of the rocket about its z axis
m = mass
p = pressure
r = radius
T_z = moments taken about the z axis of the rocket
t = time
W = weight
x,y,z = axes of a right-handed Cartesian coordinate frame; also, the distances measured along these axes

Subscripts

aft = aft tube of the launcher
c.g. = measured with respect to the simulated center of gravity of the rocket
for = forward tube of the launcher
n.e. = measured at the nozzle exit plane
0 = initial conditions

Introduction

THERE are a variety of military rockets which are launched from variable-area launch tubes. The flow of the rocket's high-temperature and high-pressure exhaust gas in these so-called "nontipoff" launch tubes is particularly complex when the flow encounters a constrictive change in the cross-sectional area. Of special concern is the possible generation of unbalanced forces on the rocket by exhaust gas which is turned upstream (which is termed blowby flow). This could influence the trajectory, once the rocket is released from its constraints and is flying free as it emerges from the forward tube. This concept is illustrated in Fig. 1. During that portion of the flight when the rocket exhausts directly into the small-diameter aft tube, it is constrained while the linear and the angular momentum of the rocket increase. Once the exit plane of the rocket nozzle reaches the change in cross section, the mechanisms which constrain the rocket (such as sabots) are released. Thus, the sabots located at the forward end of the rocket are thrown free as the nose emerges from the tube. The constraints located at the aft end are released simultaneously, so that although a considerable portion of the rocket is still in the launcher, it flies free of constraints. During this portion of the flight, a complex system of shock waves results as the exhaust gas impinges on the launcher wall and then encounters the constrictive change in cross section.

When the rocket exhausts directly into the small-diameter aft tube, the flow downstream of the nozzle exit is entirely supersonic. Weak, intersecting shock waves occur. The resultant flowfield is that for an underexpanded supersonic jet exhausting into a constant-area tube having an inside diameter which is slightly larger than the nozzle exit.[1,2]

When the rocket exhausts directly into the forward tube, the resultant flowfield may show various degrees of complexity. It is possible that flow reversal may occur when the

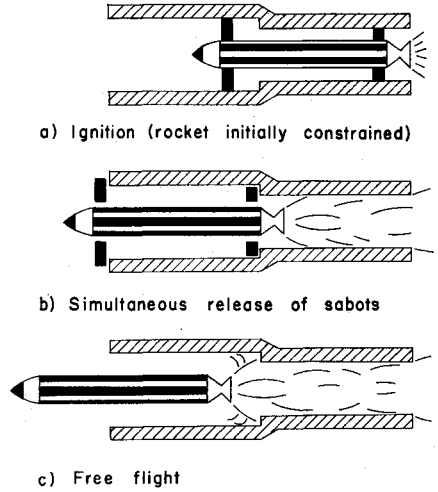

Fig. 1 Sketch of launching sequence in a constrictive launch tube.

Presented as Paper 78-115 at the AIAA 16th Aerospace Sciences Meeting, Huntsville, Ala., Jan. 16-18, 1978; submitted Feb. 3, 1978; revision received May 18, 1978.

Index categories: LV/M Aerodynamics; LV/M Testing, Flight and Ground.

*Currently Member Technical Staff, Aerodynamics Dept., Sandia Laboratories, Albuquerque, N. Mex. Member AIAA.

†Professor, Dept. of Aerospace Engineering and Engineering Mechanics. Member AIAA.

‡General Engineer, Advanced Systems Concepts.

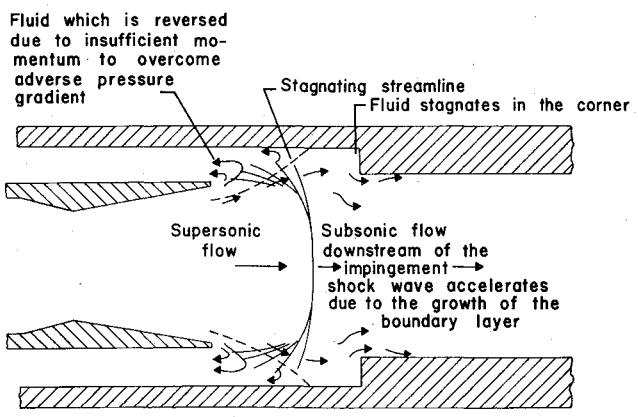

Fig. 2 A sketch of the flow model for the choked exhaust flow in a constrictive launch tube.

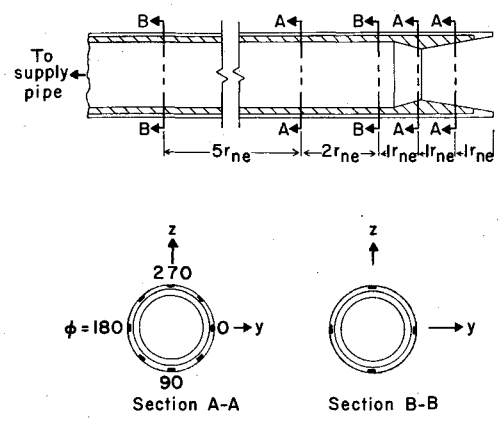

Fig. 3 Sketch of the sleeved rocket nozzle illustrating pressure orifice locations, $r_{n.e.} = 1.453$ cm (0.572 in.).

rocket exhaust either impinges directly on the step or impinges on the launcher wall prior to encountering the constriction. The analysis of this flowfield is particularly important because the exhaust gas which is deflected upstream may result in unbalanced pressure forces on the rocket. This, in turn, can cause the rocket to deviate significantly from the intended flight path once it is released from its constraints.

When the nozzle exit plane is in the forward tube, the constriction serves as a second throat for the exhaust flow. When the constrictive area ratio, i.e., the aft-tube cross-sectional area divided by the forward-tube cross-sectional area, is below a critical value, the exhaust flow is choked by the constriction. As a result, the shock wave generated as the exhaust flow impinges on the launch-tube wall is strong and the downstream flow is subsonic.

A sketch of the flowfield for which the nozzle exhaust flow becomes choked by the constriction is presented in Fig. 2. The essential features of the model include the underexpanded flow in the nozzle exit plane, the supersonic flow just upstream of the strong impingement shock wave, the subsonic flow just downstream of the impingement shock wave, the reverse, or blowby, flow (i.e., that fluid which cannot overcome the adverse pressure gradient generated by the flow impingement), the region at the base of the step where some of the fluid which has passed through the shock system stagnates, the subsonic flow at the entrance of the small-diameter aft tube, and the sonic flow at the exit plane of the small-diameter aft tube (resulting from an acceleration of the subsonic flow in the aft tube caused by the growth of the boundary layer). The latter phenomenon, described by Shapiro[3] as choking due to friction, has the net effect of reducing the allowable mass flow rate in the aft portion of the launcher.

Significant blow-by flow has been observed during flight-test programs[4] using constrictive nontipoff launch tubes for which the constrictive area ratio previously was 0.595. This is below the critical value discussed previously.

Due to difficulties inherent in obtaining flight-test data, various cold-gas facilities have been used to simulate the exhaust flowfield in the launcher. The objective of the cold-gas test programs included the determination of the parameters which govern the process by which flow downstream of the impingement shock is choked. Several test programs[5,6] have been conducted to insure the validity of correlating data obtained from rocket flight tests with those obtained from cold-gas facilities. As noted in Ref. 4, "the cold-gas simulations not only provided a realistic flow model that could be used to interpret flight test data, but the cold-gas pressure measurements correlated reasonably well with the flight test measurements."

The present experimental program was undertaken to determine the "tipoff" forces by using captive-testing techniques. This technique involves exhausting an underexpanded unheated jet of air from a stationary simulated rocket nozzle into an instrumented constrictive launch tube. The surface of the simulated rocket was also instrumented with static pressure orifices. The measured pressures were integrated to obtain the resultant forces and moments. These values were used to determine the trajectory of the "unconstrained" rocket in the forward tube as a function of time.

Experimental Program

Test Facility

The tests were conducted at the Rocket Exhaust Effects Facility located in the Experimental Aerodynamics Laboratory (EAL) of the University of Texas at Austin. Simulated rocket exhaust flows were obtained when unheated compressed air, used as the test gas, was accelerated from a high-pressure supply system through a convergent-divergent nozzle (simulated rocket) into a constrictive tube (simulated launcher). Although the test facility is capable of producing stagnation pressures as high as 7.6×10^6 N/m^2 (1100 psia), the maximum stagnation pressure at which tests were conducted in the prsent experimental program was 6.8×10^6 N/m^2 (980 psia). Since the facility is of the blowdown type, steady-state test time is limited to approximately 30 s, depending on the desired stagnation pressures.

Simulated Rocket Nozzles

A sketch illustrating the geometry of the convergent-divergent nozzle used to produce the simulated rocket exhaust is presented in Fig. 3. Throughout this paper, the distances have been nondimensionalized by $r_{n.e.}$, which is 1.453 cm (0.572 in.). The area ratio of the sleeved nozzle ($A_{n.e.}/A^* = 2.242$) may be used to determine that, from isentropic gas flow relations,[7] the nozzle exit-plane Mach number is 2.32. The machining tolerances for the nozzle were held to within ±0.003 cm (±0.001 in.).

As shown, the nozzle was sleeved so that small grooves could be milled in the outer surface to accept the stainless steel tubing used in measuring surface pressures. Since the sleeve was attached to the outer surface of the nozzle, internal stresses between the nozzle and the sleeve could be avoided, permitting the milling of as many grooves as was practical without affecting the tensile strength of the nozzle. Thus, the 32 static pressure orifices were installed on the sleeved rocket to permit direct measurement of pressures acting on its outer surface. These orifices were located at selected axial and circumferential locations to determine effects produced by the flowfield which resulted when the nozzle was exhausted into the forward tube. Presented in Fig. 3, therefore, are cross-sectional views of the particular axial locations at which the pressure taps were installed. All of the cross sections, called "stations," which contain pressure taps are located at distances equal to integer multiples of the nozzle exit radius ($r_{n.e.}$) from the nozzle exit plane. For stations with eight orifices, they are 45-deg apart. The axes are illustrated in Figs. 3 and 4. The positive y axis corresponds to $\phi = 0$ deg, where ϕ

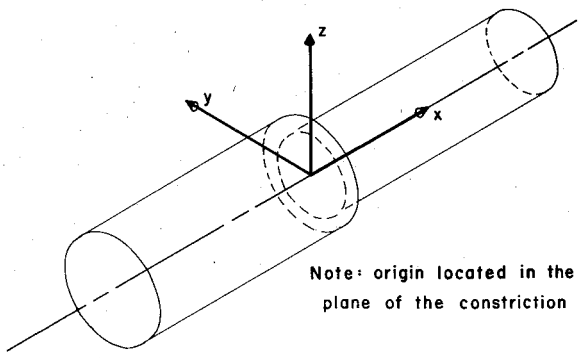

Fig. 4 The launcher-oriented coordinate system.

is the circumferential angle, which is positive when measured in the clockwise direction, looking upstream. In presenting differential pressure measurements, the xy plane contains orifices at $\phi = 0$ deg and $\phi = 180$ deg. A positive Δp indicates that the pressure was greater at the $\phi = 0$ deg orifice. Similarly, the xz plane contains orifices at $\phi = 90$ deg and $\phi = 270$ deg and a positive Δp indicates that the pressure was greater at the $\phi = 90$ deg orifice.

Simulated Launch Tube

The overall length for the launcher configuration was 83.820 cm (33.000 in.). The large-diameter forward tube (refer to Fig. 4) was 38.141 cm (15.016 in.) in length, and the small-diameter aft tube was 45.679 cm (17.984 in.). The constrictive area ratio for this launch tube was $A_{aft}/A_{for} = 0.735$.

Pressure orifices located circumferentially on the launch tube wall are designated in the same manner as those on the nozzle. To differentiate between taps located in the forward tube and those located in the aft tube, cross sections at which taps are located have been measured from the constrictive step and nondimensionalized by the nozzle exit radius $r_{n.e.}$. The taps located in the forward tube have been assigned values for which $x/r_{n.e.} < 0$. Those located in the aft tube have positive x coordinates.

Test Program

The location of the nozzle exit plane could be varied relative to the constriction, thereby simulating (in a quasisteady manner) the flowfields which result during a launching sequence. The assumption that the exhaust flow for an actual rocket launching is quasisteady is based on the fact that the velocity of the exhaust gas is much greater than either the linear velocity or the angular velocity of the rocket while it is accelerating in the tube.

In order to simulate configurations in which the centerline of the nozzle is translated and/or skewed with respect to the centerline of the launcher, the launchers were mounted onto a carriage which could be translated as well as rotated. The launch tubes could be translated along both the x and y axes and could be rotated about the z axis to vary the rocket's position with respect to the constriction and to represent movement of the rocket in the simulated vertical plane of motion. Angular rotations of the launchers were specified to be within an accuracy of ± 0.025 deg, while lateral and axial positioning of the launchers were specified to be within ± 0.013 cm (± 0.005 in.).

During initial tests, it was determined that the static pressures acting on the surface of the nozzle (i.e., the simulated rocket) would be relatively small both before and during the occurrence of blowby. To measure the surface pressures on the sleeved nozzle accurately, mercury-filled manometers were used to measure the absolute pressure acting at a particular orifice, while U-tube manometers, filled with unity-weight oil, were used to measure the differential pressures for diametrically opposed orifices. Experimental

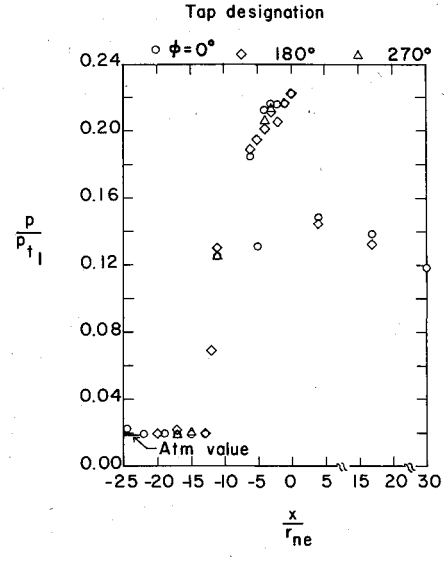

Fig. 5 The experimentally determined pressure distribution on the launcher wall, $x_{n.e.} = -12.86\ r_{n.e.}$, $y_{c.g.} = -0.0276\ r_{n.e.}$, $\theta_{c.g.} = -0.090$ deg, $p_{t1} = 5.088 \times 10^6$ N/m^2.

error associated with the visual readings taken from the manometers corresponds to a pressure error of ± 70 N/m^2 (± 0.01 psi).

Discussion of Results

As noted in the Introduction, an extremely complex flowfield may result when the rocket exhausts directly into a large-diameter forward tube. With the nozzle exit plane so located, the constriction served as a second throat for the exhaust flow. For the constrictive area ratio of the present launcher, which was 0.735, the exhaust flow was choked by the constriction. As a result, the shock wave generated as the exhaust flow impinged on the launch-tube wall was strong and the downstream flow was subsonic.

Pressure Distribution on the Launcher Wall and on the Rocket

Pressure orifices were located on the launcher wall at circumferential locations corresponding to positions 0, 180, and/or 270 deg. Thus, the static pressure distribution in the launcher during the trajectory analyses could be reasonably well defined. Also, because static pressure orifices on the launcher were located in the same plane as many of the orifices on the nozzle, the pressure variation across the annular gap between the nozzle and the launcher wall could be obtained. The static pressure distribution along the launch tube wall and the variation of the static pressures across the annular gap will be discussed now.

The experimentally determined static pressure distribution on the launcher wall is presented in Fig. 5. The nozzle exit plane was located at $x_{n.e.} = -12.86\ r_{n.e.}$. For purposes of discussion, let us compare this pressure distribution with the choked flow model of Fig. 2. For $-25.0\ r_{n.e.} < x < -12.5\ r_{n.e.}$, the pressures are essentially atmospheric, with little or no variation. There is a sudden rise in pressure from $-12.5\ r_{n.e.} < x < -10.0\ r_{n.e.}$, i.e., in the vicinity of the strong impingement shock wave. The pressure continues to increase, although not as markedly, for $-7.5\ r_{n.e.} < x < 0$ as the choked flow stagnates in the corner formed by the stepped constriction. For $0 < x < 30.0\ r_{n.e.}$, the pressure gradually decreases as the subsonic flow, which exists downstream of the normal impingement shock wave, accelerates through the aft tube.

One of the objectives of the present experimental program was to obtain information regarding the details of the flow reversal process. Of special interest was the determination of

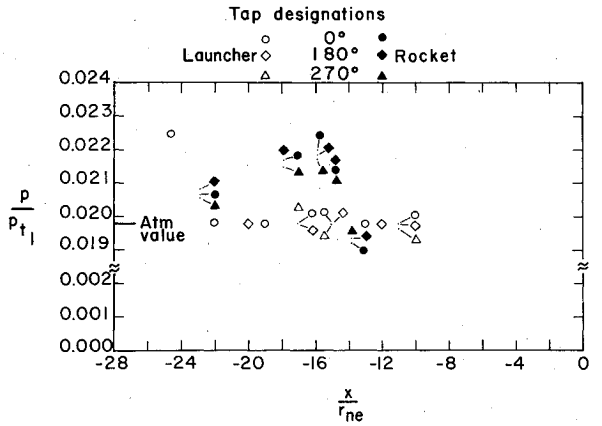

Fig. 6 Comparison between the surface pressures on the rocket and the pressures on the launcher wall (in the annular region), $x_{n.e.} = -12.86\ r_{n.e.}$, $y_{c.g.} = -0.0276\ r_{n.e.}$, $\theta_{c.g.} = -0.090$ deg, $p_{t1} = 5.088 \times 10^6$ N/m^2.

whether variations in the pressures across the annular region occurred. Presented in Fig. 6, therefore, is a comparison between the static pressure distribution measured on the wall of the launcher (open symbols) and the pressure distribution measured on the surface of the rocket (filled symbols) for the configuration of Fig. 5. (Note the expanded pressure scale of Fig. 6 compared with that of Fig. 5.) The pressures on the surface of the rocket near the exit plane (i.e., those orifices at $x = -13.86\ r_{n.e.}$) are relatively low. These relatively low pressures result because the highly curved streamlines of the flow reversal create a separation bubble on the rocket surface near the exit plane. The peak in the pressure distribution on the simulated rocket (for the orifices at $x = -15.86\ r_{n.e.}$) is attributed to a recompression of the blowby flow on the surface of the rocket. Whereas the pressures on the surface of the rocket vary considerably in the axial direction for $-24.0\ r_{n.e.} < x < -12.86\ r_{n.e.}$, the pressures on the launcher wall in this region are relatively constant. It should be noted here that the accuracy of the static pressure measurements on the surface of the nozzle is considerably greater than that of the launcher measurements. However, within the range of accuracy of the measurements, it may be generally concluded that there are significant differences between the surface pressure on the rocket and the pressures on the launcher wall.

Trajectory Simulation

A detailed sketch of the coordinate system used in the trajectory simulation to locate the rocket in the forward tube is shown in Fig. 7. Note that, even though the xy coordinate system is defined relative to the launch tube (see Fig. 4), the rocket remains fixed and the launcher is moved in the Rocket Exhaust Effects Facility. In order to properly simulate the gravity drop of the rocket, gravity was assumed to act in the negative y direction of the launcher coordinate frame. A rotation of the launcher about its z axis simulated the motion caused by pitching moments acting on the rocket. Yawing moments, rolling moments, and offset positions along the z coordinate direction were not simulated in the present test program due to the difficulty in maintaining alignment control. Thus, the centerline of the rocket and the centerline of the launcher remained coplanar throughout the test program. As shown in the figure, positive values of the pitching moments correspond to a counterclockwise rotation of the launcher about its z axis. This rotation has been denoted by $\theta_{c.g.}$, the angle between the centerline of the launcher and the nozzle. Note also that positive values of the offset, denoted by $y_{c.g.}$ in the figure, correspond to the perpendicular distance between the simulated center of gravity of the rocket and the centerline of the launcher, as measured along the y axis of the launcher coordinate frame. The simulated center

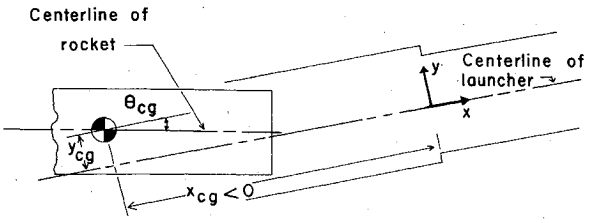

Fig. 7 Sketch of the simulated rocket in the forward launch tube with respect to the launcher-oriented coordinate system (not to scale).

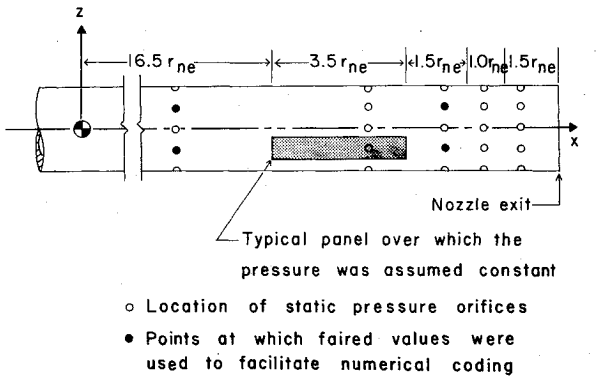

Fig. 8 Sketch of the sleeved nozzle illustrating the static-pressure orifices and a typical panel used in calculating the forces acting on the rocket.

of gravity for the rocket was located a distance of $24.0\ r_{n.e.}$ from the nozzle exit plane. It should be re-emphasized at this point that the rocket was actually stationary for all tests, and that to simulate the calculated positions of the rocket in the launcher, the launcher was translated and rotated to the desired positions.

Because there were only 32 pressure orifices, the pressure distribution over the surface of the rocket could only be approximated by the experimentally determined pressures. For purposes of numerical calculations, therefore, the static pressure measured at a particular orifice was assumed to be constant over a finite surface area of the simulated rocket during the time interval for which the equations of motion were integrated. The dimensions of a typical "panel" over which the pressures were assumed constant are illustrated in Fig. 8. Each panel is located such that its boundaries lie midway between the orifice at a particular station and the orifices immediately upstream and immediately downstream of that particular station. The downstream boundary for the panels located nearest the nozzle exit was taken to be the nozzle exit plane. The upstream boundary for the panels associated with the orifices located a distance of $10.0\ r_{n.e.}$ from the nozzle exit plane (see Fig. 3 and Fig. 8) coincides with the assumed position of the center of gravity location. From the dimensions of each panel, the pressure measured at the corresponding orifice could be used to calculate the force acting on that particular panel. Taking into account the total effect of all forces and moments thus determined, the numerical values of pitch, pitch rate, etc., could be easily calculated.

In order to integrate the individual pressure measurements so that the forces, the moments, and the resultant rocket motion could be calculated, an elementary numerical code was developed. The code was used to calculate the trajectory of a hypothetical rocket. The hypothetical rocket was characterized as follows:

Thrust $= 4.45 \times 10^4$ N (10,000 lb$_f$)
Weight $= W = 1.11 \times 10^3$ N (250 lb$_f$)
Inertia (about z axis of launcher) $= I_z = 1.00$ m^2-kg
$= 23.83$ lb$_m$-ft^2.
Distance from nozzle exit plane to rocket c.g. $= 24.0\ r_{n.e.}$

These parameters were used in the integrated equations of motion to predict the location of the center of gravity of the simulated rocket during the trajectory analysis.

The numerical code which was developed to track the rocket's center of gravity in the forward portion of the launch tube employs the classical equations of dynamics

$$\sum T_z = I_z \ddot{\theta}_{c.g.} \tag{1}$$

for the simulated angular acceleration and

$$\sum F_y - W = m\ddot{y}_{c.g.} \tag{2}$$

$$\sum F_x = \text{thrust} = -m\ddot{x}_{c.g.} \tag{3}$$

for the linear acceleration of the rocket along the y and x axes, respectively. The static pressures measured on the simulated rocket were integrated to determine the forces which make up the ΣF_y term. The differential pressures which were measured on the simulated rocket for the cold-gas flows were applied directly to the full-scale vehicle to calculate the trajectories. This represents a major assumption in these trajectory simulations. Since static pressures have never been measured on the surface of a rocket during a flight test, there is no measure of the validity of this assumption. The weight of the rocket being simulated remains essentially constant during the finite time interval over which the preceding equations are integrated. The forces acting on the system are also assumed to remain constant during the time interval Δt.

To calculate the angular, lateral, and axial positions of the rocket, successive integration of the preceding equations yields:

$$\theta_{c.g.} = (\Sigma T_z / 2I_z)(t^2 - 2tt_0 + t_0^2) + \dot{\theta}_0 \Delta t + \theta_0 \tag{4}$$

$$y_{c.g.} = [(\Sigma F_y - W)/2m](t^2 - 2tt_0 + t_0^2) + \dot{y}_0 \Delta t + y_0 \tag{5}$$

$$x_{c.g.} = (-\text{thrust}/2m)(t^2 - 2tt_0 + t_0^2) + \dot{x}_0 \Delta t + x_0 \tag{6}$$

where $\theta_{c.g.}$, $y_{c.g.}$, and $x_{c.g.}$ are as shown in Fig. 7.

The initial conditions used to start the trajectory calculations were determined as follows. The trajectory simulation was initiated with the exit plane of the rocket located at the constrictive step. The velocity of the rocket at the instant the nozzle exit plane passed the constrictive step (which is $\dot{x}_0$, the initial velocity as the rocket first flies free of its constraints) was assumed to be 42.9 m/s (140.9 fps). The centerline of the rocket and the centerline of the launcher are assumed to be collinear since the sabots which support and center the rocket while it is in the aft portion of the launcher are released as it enters the forward tube. Therefore, with the nozzle exit plane located at the constrictive step, the initial conditions are

$$\theta_0 = 0 \qquad \dot{\theta}_0 = 0$$

$$y_0 = 0 \qquad \dot{y}_0 = 0$$

$$x_0 = -24.0\, r_{n.e.} \qquad \dot{x}_0 = -42.9 \text{ m/s} (-140.9 \text{ fps})$$

During the initial time step, it was assumed that massive blowby would not occur. Thus, the only forces acting on the rocket at this position would be thrust and weight. As a result, the rocket undergoes a lateral translation in the negative y direction (simulated gravity drop), an axial translation in the negative x direction (due to thrust), but no angular rotation. By moving the launcher carriage, the rocket could be placed in the desired position relative to the launch tube. Flow was then

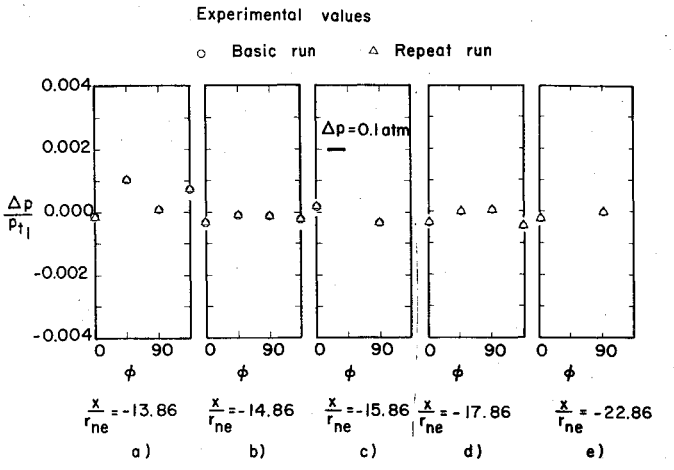

Fig. 9 The experimentally determined pressure distribution on the surface of the sleeved nozzle, $x_{n.e.} = -12.86\ r_{n.e.}$, $y_{c.g.} = -0.0276\ r_{n.e.}$, $\theta_{c.g.} = -0.090$ deg, $p_{t1} = 5.088 \times 10^6$ N/m^2 (738 psia).

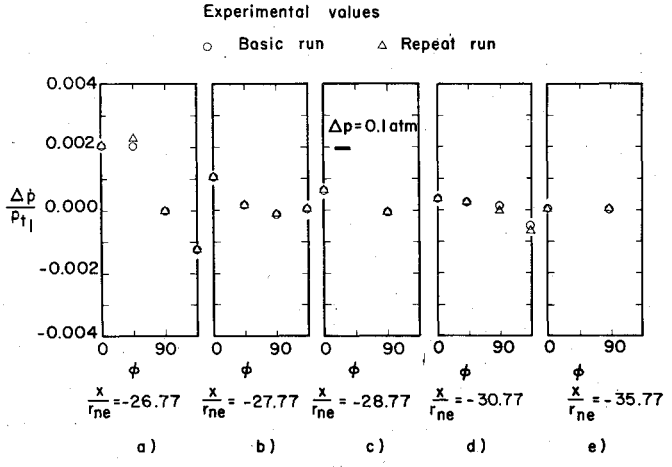

Fig. 10 The experimentally determined pressure distribution on the surface of the sleeved nozzle, $x_{n.e.} = -25.77\ r_{n.e.}$, $y_{c.g.} = -0.0997\ r_{n.e.}$, $\theta_{c.g.} = +0.472$ deg, $p_{t1} = 5.088 \times 10^6$ N/m^2 (738 psia).

exhausted through the nozzle into the tube in order to determine the forces and moments which act on the rocket during the next time interval. Thus, using the values of x, $\dot{x}$, y, $\dot{y}$, θ, and $\dot{\theta}$ calculated for the end of one time interval as the initial conditions to be used for the next time interval, the path of the rocket could be determined during that "next" time interval. The procedure was continued until the nozzle exit plane exited the forward end of the launcher.

For the present experimental program, two trajectory simulations were conducted. Repeat tests were performed for both test simulations to obtain a "measure" of the uncertainty of the data. However, repeat runs for the initial location of the simulated rocket were not made. Since the only forces acting on the rocket are the thrust and the weight, there was "no uncertainty" in the trajectory during the initial time. Presented in Figs. 9 and 10 are the experimentally determined differential pressure distributions on the surface of the sleeved nozzle. Note that $x/r_{n.e.}$ designates the group of orifices at a particular section as measured from the constrictive step. Data are presented for only one trajectory simulation since the two trajectories were essentially the same. Data are presented for nozzle exit locations of $x_{n.e.} = -12.86\ r_{n.e.}$ and $x_{n.e.} = -25.77\ r_{n.e.}$. The nozzle stagnation pressure of $p_{t1} = 5.088 \times 10^6$ N/m^2 (738 psi) was used for each test in the simulation.

The data of Figs. 9 and 10 indicate that the highest differential pressures occur at those orifices nearest the nozzle

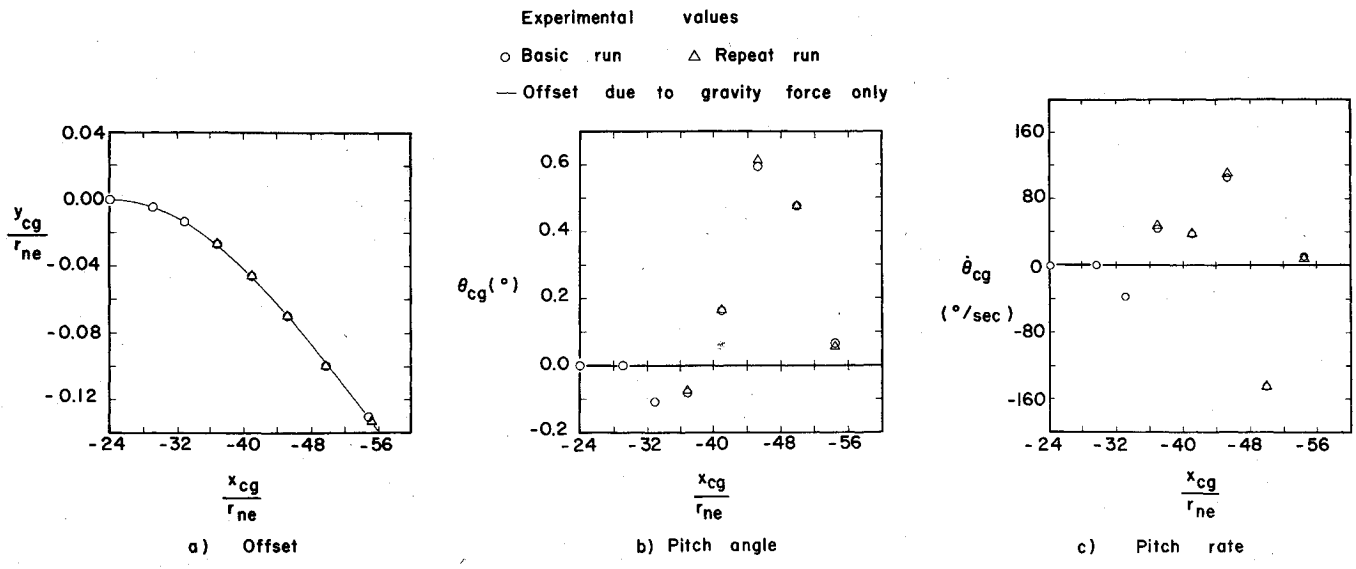

Fig. 11 The experimentally determined location of the rocket in the forward tube.

exit plane. The large pressure differentials acting on the rocket are the result of the large gradients which occur because the supersonic exhaust flow is reversed in a very short distance. Due to the relatively large distance between the simulated center-of-gravity position and the nozzle exit plane, it may be expected that these asymmetric pressures would seriously influence the resultant pitch angle and pitch rate. For those orifices farther away from the nozzle exit plane (which are nearer the forward end of the launch tube), the pressure differential decreases due to the requirement that the static pressure in the annular region (i.e., the region between the rocket and the launcher wall) must eventually equal the ambient pressure. No clearly discernible pattern has been found in the pressure distributions. However, comparison of differential pressures measured at particular values of $x/r_{n.e.}$ for each nozzle exit location indicates that an oscillatory pressure field occurs as the rocket is moved farther away from the constriction. The data from the xy plane indicate that the differential pressure becomes more negative (i.e., the pressures at the $\phi = 180$-deg orifice is larger than that at the $\phi = 0$-deg orifice) as $x_{n.e.}$ becomes more negative, but then reverses and becomes positive. The remaining data show similar variations. For the values of offset and cant for these configurations (which are tabulated in the figures), the maximum differential pressure occurred at different locations on the rocket. Therefore, the oscillatory nature of the data indicates that, for the lower values of $x_{n.e.}$, forces are developed which result in pitching moments which tend to move the rocket back toward the centerline of the launcher. These forces, however, produce large angular velocities as the rocket moves down the launcher. This will become more apparent from the trajectory plots, which are presented in the subsequent figures.

Because the magnitudes of the pressure differentials are very sensitive to the configuration geometry (nozzle exit location, rocket orientation, and launcher geometry) and because they vary from station to station, it is clear that the annular blowby phenomena are complex and highly configuration-dependent.

The calculated values of $y_{c.g.}/r_{n.e.}$, $\theta_{c.g.}$, and $\dot{\theta}_{c.g.}$ are presented as a function of $x_{c.g.}/r_{n.e.}$ in Fig. 11. These data correspond to a trajectory simulation for which the initial time step was taken to be $\Delta t = 8.84 \times 10^{-3}$ s. Each subsequent time step was arbitrarily taken to be $\Delta t = 6.00 \times 10^{-3}$ s. For Fig. 11a, the experimentally determined offset, $y_{c.g.}/r_{n.e.}$, is compared to the offset which would occur if the only force acting on the rocket were gravity. From this comparison, it is evident that the occurrence of blowby had no pronounced effect on the lateral displacement. The data presented in Fig. 11b for $\theta_{c.g.}$, and in Fig. 11c for $\dot{\theta}_{c.g.}$ indicate, however, that the differential surface pressures resulting from massive blowby had a marked effect on the pitch and on the pitch rate. As evident in the data presented in the figures, large oscillatory variations in the angular motion parameters were recorded. Therefore, these data compare qualitatively to data obtained in actual flight tests (see Ref. 8). However, because the differential pressures measured on the scale-model, simulated rocket during the cold-gas tests were applied directly to the full-scale, hypothetical rocket, the reader is cautioned not to overemphasize the absolute values of the angular displacement or of the angular velocity presented in these figures.

Concluding Remarks

An experimental program has been conducted in which an underexpanded jet of air was exhausted into a constrictive launch tube in order to investigate the effects of massive blowby on the simulated rocket. For the range of flow conditions and geometric configurations considered in the present program, the following conclusions are made.

1) Once the exhaust flow in the launch tube was choked and massive blowby occurred, relatively large asymmetric pressure differentials were measured on the surface of the simulated rocket. Experiments have shown that pressure differentials existed on the rocket even though the axis of the rocket and the axis of the launcher were collinear. Thus, the asymmetric pressures were a direct result of blowby, since asymmetry in the launcher-nozzle configuration was controlled within small tolerances.

2) A simple numerical code was developed in order to analyze the effect of the pressure distribution, integrated over the surface of the simulated rocket, on the simulated trajectories. The lateral displacement (i.e., $y_{c.g.}/r_{n.e.}$) was found to be relatively insensitive to forces and moments produced by massive blowby. However, the occurrence of massive blowby had a substantial effect on the angular motion variable considered in the present program, $\theta_{c.g.}$. The experimentally determined pitch and the pitch rate were observed to consist of large oscillatory variations as the rocket moved down the launcher.

Acknowledgments

This work was supported by the U.S. Army Missile Research and Development Command through Contract DAAK 40-73-C-1016.

References

[1] Fabri, J. and Seistrunck, R., "Supersonic Air Ejectors," *Advances in Applied Mechanics*, Vol. V, Academic Press, New York, 1958, pp. 1-34.

[2] Batson, J. L. and Bertin, J. J., "Experimental Study of Flowfield Produced when an Underexpanded Rocket Exhausts into a Cylindrical Tube," AIAA Paper 73-1227, Las Vegas, Nev., Nov. 1973.

[3] Shapiro, A. H., *The Dynamics and Thermodynamics of Compressible Fluid Flow*, Ronald Press, New York, 1953.

[4] Bertin, J. J. and Batson, J. L., "Experimentally Determined Rocket Exhaust Flowfield in a Constrictive Tube Launcher," *Journal of Spacecraft and Rockets*, Vol. 12, Dec. 1975, pp. 711-717.

[5] Bertin, J. J. and Batson, J. L., "Comparison of Cold-Gas Simulations and Rocket-Launch Data for Constrictive Launchers," *Journal of Spacecraft and Rockets*, Vol. 13, Nov. 1976, pp. 684-691.

[6] Bertin, J. J., Cribbs, D. W., Barnette, D. W., and Booker, D. L., "Onset of Massive Blowby, a Comparison of Cold-Gas Simulations and Flight Tests," AIAA Paper 78-16, AIAA 16th Aerospace Sciences Meeting, Huntsville, Ala., Jan. 1978.

[7] Ames Research Staff, "Equations, Tables, and Charts for Compressible Flow," NACA Rept. 1135, 1953.

[8] "Non-Tipoff Tube Launcher Flight Test Program," LTV Aerospace Corp., Michigan Div., 7-52100/3R-61, Dec. 1973.